LAWRENCE
LIVERMORE
NATIONAL
LABORATORY

LLNL-JRNL-609712

Reductive Dechlorination by an Anaerobic Consortium during Bioenhanced PCE Dissolution: Model Validation and Sensitivity Analysis

M. Chen, L. M. Abiola, B. K. Amos, E. J. Suchomel, K. D. Pennell, F. E. Loeffler, J. A. Christ

January 7, 2013

Journal of Contaminant Hydrology

Disclaimer

Reductive Dechlorination by an Anaerobic Consortium during Bioenhanced PCE Dissolution: Model Validation and Sensitivity Analysis

Mingjie Chen[1], Linda M. Abriola[2], Benjamin K. Amos[3], Eric J. Suchomel[4], Kurt D. Pennell[2], Frank E. Löffler[5,6], and John A. Christ[7*]

[1]Atmospheric, Earth and Energy Division, Lawrence Livermore National Laboratory, Livermore, CA 94550
[2]Department of Civil and Environmental Engineering, Tufts University, Medford, MA 02155
[3] Geosyntec Consultants, Kennesaw, GA 30144
[4] Geosyntec Consultants, Oakland, CA 94612
[5] Department of Civil and Environmental Engineering, University of Tennessee, Knoxville, TN 37996
[6] Department of Microbiology, University of Tennessee, Knoxville, TN 37996
[7] Department of Civil and Environmental Engineering, US Air Force Academy, CO 80840.

For Submission to Journal of Contaminant Hydrology

[*]Corresponding author

USAF Academy
Department of Civil and Environmental Engineering
2354 Fairchild Drive, Suite 6J-159
USAF Academy CO 80840-6232
Phone: (719) 333-3150
Fax: (719) 333-9102

Email:john.christ@usafa.edu

Abstract

Reductive dechlorination catalyzed by organohalide-respiring bacteria is often considered for remediation of non-aqueous phase liquid (NAPL) source zones due to cost savings, ease of implementation, regulatory acceptance, and sustainability. Despite knowledge of the key dechlorinators, an understanding of the processes and factors that control NAPL dissolution rates and detoxification (i.e., ethene formation) is lacking. A recent column study demonstrated a 5-fold cumulative enhancement in tetrachloroethene (PCE) dissolution and ethene formation (Amos *et al*., 2009). Spatial and temporal monitoring of key geochemical and microbial (i.e., *Geobacter lovleyi* and *Dehalococcoides mccartyi* strains) parameters in the column generated a data set used herein as the basis for refinement and testing of a multiphase, compositional transport model. The refined model is capable of simulating the reactive transport of multiple chemical constituents produced and consumed by organohalide-respiring bacteria and accounts for substrate limitations and competitive inhibition. Parameter estimation techniques were used to optimize the values of sensitive microbial kinetic parameters, including *maximum utilization rates*, *biomass yield coefficients*, and *endogenous decay rates*. Comparison and calibration of model simulations with the experimental data demonstrate that the model is able to accurately reproduce measured effluent concentrations, while correctly delineating growth of dechlorinators and reductive dechlorination kinetics throughout the column. Sensitivity analyses performed on the optimized model parameters indicate that the rates of PCE and *cis*-1,2-dichloroethene (*cis*-DCE) transformation and *Dehalococcoides* growth will govern bioenhanced dissolution, as long as electron donor (i.e., hydrogen flux) is not limiting. Dissolution enhancements are shown to be strongly influenced by the accumulation of *cis*-DCE, which inhibits reductive dechlorination to ethene, as well as column length and flow rate (i.e., column residence time). If *cis*-DCE

inhibition was neglected, the model over-predicted ethene production nine fold, while reductions in residence time (i.e., a two-fold decrease in column length or two-fold increase in flow rate) resulted in a more than 70% decline in ethene production. These results demonstrate that spatial and temporal microbial community dynamics and activity must be understood to model, predict, and manage bioenhanced NAPL dissolution.

1. Introduction

Chlorinated solvents (e.g., tetrachloroethene [PCE], trichloroethene [TCE]), are widely used in industrial processes, and at military installations and government facilities, and have often been released as dense non-aqueous phase liquids (DNAPLs). DNAPL dissolution, whether from pools retained above or within low-permeability strata or from residual saturation ganglia trapped in the porous soil or rock matrix, creates a persistent source of groundwater contamination. In the past two decades, numerous remediation technologies have been developed to treat DNAPL source zones; however, the ability of a single technology to completely remove or destroy all DNAPL mass and reduce dissolved-phase contaminant concentrations below drinking water standards is limited. Among potential *in situ* remediation technologies, microbial reductive dechlorination has emerged as an attractive DNAPL source zone remedy (Da Silva et al., 2006; Sleep et al., 2006; Schaefer et al., 2010), and as a source zone polishing step to control residual contaminant concentrations following aggressive physicochemical treatment (Mravik et al., 2003; Ramsburg et al., 2004; Christ et al., 2005). During source zone bioremediation, microbial activity lowers dissolved-phase contaminant concentrations, thereby increasing the driving force for contaminant dissolution from the DNAPL to the aqueous phase, a process commonly referred to as bioenhanced dissolution (Yang and McCarty, 2000; Cope and Hughes, 2001; Yang and McCarty, 2002; Adamson et al., 2003; Sleep et al., 2006; Glover et al., 2007;

Amos et al., 2008). While dissolution enhancements may lead to short term increases in dissolved phase *cis*-DCE concentrations, the overall source longevity and associated cleanup times decrease, potentially resulting in reduced long-term risk.

Results obtained from batch, column, and aquifer cell experiments indicate that the extent of DNAPL dissolution enhancement due to bioactivity can vary widely, from a negligible effect to a more than 20-fold increase (e.g. Carr et al., 2000; Yang and McCarty, 2000; Cope and Hughes, 2001; Sleep et al., 2006; Amos et al., 2008, 2009; Schaefer et al., 2010; Philips et al., 2011). This variability in dissolution enhancement has been attributed to several factors, including differing microbial populations, electron donor limitations, competitive and threshold inhibitions, and competitor populations (e.g., methanogens), as well as changing flow conditions due to gas formation, microbial growth, and experimental design. While bench-scale experiments provide excellent demonstrations of the conditions leading to bioenhanced DNAPL dissolution (e.g., Amos et al., 2009; Schaefer et al., 2010), their use as a design tool for treatment applications in the field is limited. Numerical simulators provide a complementary tool that allows for more efficient assessment of individual parameters and inter-related processes impacting microbial activity, guiding future efforts to understand and optimize *in situ* bioenhanced dissolution.

Prediction of microbial-enhanced DNAPL dissolution requires a model that quantifies inter-relationships between dechlorination and mass transfer processes. A number of models capable of simulating organohalide respiration kinetics have been presented in the literature that incorporate electron donor flux (i.e., fermentation) and competition (i.e., methanogenesis) (e.g. Bagley, 1998; Fennell and Gossett, 1998; Lee et al., 2004; Yu et al., 2004, 2005, Becker, 2006; Huang and Becker, 2009; Becker and Seagren, 2009; Haest et al., 2010; Kouznetsova et al., 2010;

Sabalowsky and Semprini, 2010; Huang and Becker, 2011). These models, however, are limited to the simulation of dechlorination in batch reactors or single-phase, aqueous systems. While several models that include both dechlorination and dissolution have been presented (Chu et al., 2003; Widdowson, 2004; Hammond et al., 2005; Chambon et al., 2010), those models have only been applied to simplified systems (e.g., no dissolution) and thus, have not considered the potential influence of a diminishing DNAPL mass on the temporal and spatial evolution of the mobile aqueous phase flow and microbial activity. A number of multi-phase, multi-component simulators have been adapted to model organohalide respiration in DNAPL source zones (Delshad et al., 1996; Abriola et al., 1997; Rathfelder et al., 2000; Willis and Shoemaker, 2000; Battisstelli, 2004; Clement et al., 2004). Only a very few studies (Christ and Abriola, 2006; Becker and Seagren, 2009), however, have explored dissolution enhancements due to microbial activity. Christ and Abriola (2006) adapted a multiphase compositional simulator (e.g., MISER – Michigan Subsurface Environmental Remediation Simulator) to incorporate dynamic interphase mass transfer, non-linear dechlorination kinetics, microbial inhibition, and competition in a framework that is capable of simulating two-dimensional non-uniform source zones. Their comparisons to available data indicated that the model was capable of capturing effluent concentrations consistent with bioenhanced dissolution. However, these data were limited to the PCE-to-*cis*-DCE dechlorination step, and did not provide the information necessary to fully calibrate and validate the model. The resulting simulations were thus, hypothetical in nature and provided limited insight into the fundamental factors controlling bioenhanced dissolution efficacy within a source zone, including conditions leading to incomplete or stalled reductive dechlorination, a frequent limitation of bioremediation during field application.

A continuous-flow column experiment (Amos et al., 2009), instrumented to quantify aqueous phase constituent concentrations (e.g., organic acids, PCE, TCE, *cis*-DCE, vinyl chloride [VC], ethene) and the distributions of key dechlorinating populations (i.e., *Geobacter lovleyi* strain SZ [GEOSZ] and *Dehalococcoides mccartyi* [DHC]) along the length of the column, provides a novel, high resolution data set to elucidate factors controlling bioenhanced dissolution and reductive dechlorination within DNAPL source zones and associated down-gradient plume regions. In this work, the experimental results of Amos et al. (2009) are compared to model simulations to: (i) examine the ability of a state-of-the-art mathematical model to simulate spatial and temporal changes in bioenhanced dissolution and reductive dechlorination; (ii) quantify microbial transformation, utilization, and growth rates using parameter estimation techniques; and (iii) identify and assess system parameters most influential in controlling bioenhanced dissolution and reductive dechlorination within a DNAPL source zone. Knowledge gained from the analysis of the relative importance of system parameters to each step of the dechlorination process provides additional insight into dechlorination and bioenhanced dissolution mechanisms and may serve to direct future research, and guide effective implementation of bioenhanced dissolution strategies at the field scale.

2. Methodology

2.1 Column experiment

Bioactive column data were primarily obtained from Amos et al. (2009), in which a 4.8 cm (inside diameter) × 60 cm (length) borosilicate glass column was constructed with 11 glass sampling ports located on alternating sides of the column at 5 cm intervals to allow for monitoring of aqueous phase constituents and microbial populations in space and time (Figure 1).

The column was packed with sterile Federal Fine Ottawa sand under anoxic, water-saturated conditions. The column was uniformly inoculated with a non-methanogenic PCE-to-ethene dechlorinating microbial consortium (BDI-SZ) that contained DHC, a *Dehalobacter* sp. (DHB), and GEOSZ. The porosity of the packed column was approximately 0.37 (Table 1), yielding a total pore volume of 407 mL. During the first stage (days 1 – 4) of the experiment, a reduced mineral salts medium without growth substrates was flushed through the column in an upflow mode at a rate of 0.25 mL/min for 3.3 pore volumes. Following this microbial elution phase, a 10-cm long NAPL source zone was established by injecting an anoxic NAPL containing 0.25:0.75 (mol:mol) PCE in hexadecane into the first 10-15 cm of the column (upflow mode), after which the flow direction was reversed and a reduced medium was introduced from the top of the column (downflow mode) to displace mobile NAPL from the pore space. The resulting source zone area contained approximately 14 mL of PCE-containing NAPL that was uniformly distributed over the first 10 cm of the column as entrapped droplets and ganglia (average initial saturation = 0.21), which transitioned (10-15 cm) to a NAPL-free, down-gradient plume region over the remainder of the column (15-60 cm).

Following establishment of the NAPL source zone, a reduced medium amended with 20 mM lactate was delivered in an upflow mode at a flow rate of 0.25 mL/min, corresponding to a residence time of 1.1 days. The flow was temporarily interrupted after 16.8 pore volumes (19 days) for 22 hours, and subsequently reduced to 0.1 mL/min after 21.6 pore volumes (24 days) to increase the solution residence time within the column. Effluent samples were collected every 1 to 3 days and side-port samples were collected periodically (after 9, 14, 20, 28 and 30 pore volumes) to monitor for chlorinated ethenes, pH, organic acids, and dechlorinating bacteria. After PCE was completely depleted from the mixed-NAPL (ca. day 55), a 1.1 pore volume pulse

(450 mL) of reduced medium amended with VC was injected into the column. This final stage of the experiment was used to determine if the BDI-SZ consortium was capable of complete dechlorination of VC to ethene following depletion of polychlorinated ethenes.

During the first 4 days of NAPL dissolution, effluent PCE concentrations were near equilibrium (Figure 2), which is consistent with the delay in the onset of lactate fermentation, suggesting that PCE dechlorination was limited by the absence of direct electron donors (i.e., hydrogen and acetate). Between days 4 and 12, the total chlorinated ethenes concentration (PCE, *cis*-DCE and VC) approached the system equilibrium value, indicating that while dechlorination was occurring, enhancements in dissolution due to bioactivity were negligible. Amos et al. (2009) hypothesized that this phase of the experiment represented an acclimatization period, in which the microorganisms reached sufficient numbers in the NAPL-contaminated source zone region to facilitate enhancing dissolution. After day 12, a rapid increase in *cis*-DCE formation was observed, consistent with bioenhanced dissolution. A spike in VC was observed after the flow interruption on day 19, but VC concentrations returned to previous levels when flow was resumed. This observation suggests that the column residence time was insufficient for the *cis*-DCE to VC dechlorination step. After the flow rate was reduced from 0.25 to 0.1 mL/min on day 24, VC concentrations continued to increase until day 45, when the PCE in the column was completely depleted and ethene production began. The observation that ethene formation was minimal until after day 45 suggests that VC to ethene dechlorination was inhibited by high *cis*-DCE concentrations (e.g., Yu et al., 2005). These results, when combined with side-port sample data, provide a comprehensive data set to support: (i) conceptual and mathematical model development and validation; and (ii) the subsequent investigation of the influence of residence

time and *cis*-DCE formation on complete detoxification of PCE to ethene in a NAPL source zone and associated plume region.

2.2 Model development

Numerical simulations were performed using a modified version of MISER (Christ and Abriola, 2006), a two-dimensional, finite element immiscible multiphase, multi-component transport simulator originally developed for soil vapor extraction and bioventing (Abriola et al., 1997; Rathfelder et al., 2000). Christ and Abriola (2006) modified the original biodegradation module in MISER to incorporate metabolic reductive dechlorination of multiple contaminants by multiple microbial populations in a DNAPL source zone. The detailed mathematical formulation, including dechlorination kinetics, and its numerical implementation have been presented previously (Abriola et al., 1997; Christ and Abriola, 2006). The main features of the modified MISER model are described below.

2.2.1 Governing equations

The NAPL phase is assumed to be discontinuous and immobilized by capillary forces, while the aqueous phase is assumed to be mobile and influenced by changes in relative permeability as the NAPL dissolves. Phase mass balance equations are given as:

$$\phi \frac{\partial}{\partial t}\left(\rho_w S_w\right) = \nabla \cdot \left(\rho_w q_w\right) + \sum_c E_{wo}^c + \sum_c B_w^c + Q_w \tag{1a}$$

$$\phi \frac{\partial}{\partial t}\left(\rho_o S_o\right) = -\sum_c E_{wo}^c \tag{1b}$$

where, $q_w = \phi S_w V_w = -\frac{k k_{rw}}{\mu_w}\left(\nabla P_w - \rho_w g\right)$ is the aqueous phase flux computed by the modified form of Darcy's law, ϕ is the matrix porosity (-), ρ_w and ρ_o are the aqueous and NAPL phase

density (M/L^3), S_w and S_o are the aqueous and NAPL phase saturation (-), and E_{wo}^c, B_w^c, Q_w are the interphase mass exchange, bioreaction, and source/sink terms (M/L^3-t), respectively. Eq. (1a) relates the change in aqueous phase mass to the aqueous phase advective flux (first term), mass transfer to the organic phase (second term), biological reactions (third term), and source/sinks (fourth term). Mass transferred from the aqueous phase accumulates in the organic phase as shown in equation 1b.

Within the aqueous phase, the mass balance for each chemical component *c* is expressed:

$$\phi \frac{\partial}{\partial t}\left(S_w C_w^c\right) + \phi \nabla \cdot S_w \left(v_w C_w^c - D_w^c \nabla C_w^c\right) = E_{wo}^c + B_w^c \tag{2}$$

where C_w^c is the concentration of component *c* in the aqueous phase (M/L^3), v_w is the pore water velocity (q_w/ϕ) (L/t), D_w^c is the aqueous phase hydrodynamic dispersion coefficient for component *c* (L^2/t), and all other parameters are as given previously. Note that since no mass transport occurs within the NAPL phase, there is no corresponding equation for immobile NAPL.

2.2.2 PCE Dissolution

PCE mass transfer from entrapped NAPL to the aqueous phase (i.e., dissolution) is modeled using a linear driving force expression to approximate the concentration gradient between the surface of the NAPL and the bulk aqueous phase:

$$E_{wo}^{PCE} = k_{wo}^{PCE}\left(C_{wo}^{PCE-e} - C_w^{PCE}\right) \tag{3}$$

where C_{wo}^{PCE-e} is the aqueous concentration in equilibrium with the mixed NAPL, as determined by Raoult's law and the assumption of ideal fluid behavior (i.e., activity coefficients equal one) (Schwarzenbach et al., 2003), and C_w^{PCE} is the bulk aqueous phase PCE concentration. The lumped mass transfer coefficient, k_{wo}^{PCE}, is the product of the mass transfer coefficient and

interfacial area per unit volume of porous media. This lumped mass transfer coefficient is typically modeled using a Sherwood number correlation (e.g., Miller et al., 1990; Powers et al., 1992, Imhoff et al., 1994). Given the conditions of the column experiment, the modified Sherwood number correlation for transient dissolution developed by Powers et al. (1994) was judged most appropriate:

$$Sh = 4.13 Re^{0.598} \left(\frac{d_{50}}{d_M} \right)^{0.673} U_i^{0.369} \left(\frac{S_o}{S_o^0} \right)^{\alpha} \tag{4}$$

where the Reynolds number is defined as $Re = q_w \rho_w d_{50} / \mu_w$, d_{50} / d_M represents the median grain size normalized by a "medium" sand grain diameter (d_M) of 0.05 cm, as defined by the U.S. Department of Agriculture (Driscoll, 1986), $U_i = d_{60} / d_{10}$ is the uniformity index, and the fitting parameter $\alpha = 0.518 + 0.114\left(d_{50} / d_M\right) + 0.1 U_i$. Here, d_i denotes the grain size that is *i* % of finer particles by weight, and S_o^0 and S_o are the initial and transient NAPL saturations, respectively. Rearranging the modified Sherwood number, $Sh = k_{wo}^{PCE} d_{50}^2 / D_L$ (Miller et al., 1990) gives:

$$k_{wo}^{PCE} = 4.13 \frac{D_L}{d_{50}^2} Re^{0.598} \left(\frac{d_{50}}{d_M} \right)^{0.673} U_i^{0.369} \left(\frac{S_o}{S_{o0}} \right)^{\alpha} \tag{5}$$

Note that k_{wo}^{PCE} is a function of Reynolds number and hence, of the aqueous phase velocity. During flow interruption, the velocity is zero and Eq. (5) is no longer applicable. In this case, the lumped mass transfer coefficient is assumed to be a constant, estimated by fitting measured data.

2.2.3 Kinetic model for reductive dechlorination

Here the conceptual model presented in Christ and Abriola (2006), which incorporates PCE to *cis*-DCE (via TCE as intermediate) followed by *cis*-DCE to ethene (via VC as intermediate) reductive dechlorination reactions, was adapted for the BDI-SZ experimental

conditions. The PCE-to-ethene-dechlorinating consortium BDI-SZ contains populations (FER) that convert lactate to acetate and propionate and increase hydrogen flux, thus providing electron donors for the organohalide-respiring populations responsible for PCE to ethene reductive dechlorination. Methanogens are absent from the BDI-SZ consortium ([*Amos et al.*, 2007b; *Amos et al.*, 2008; *Amos et al.*, 2009; *Ritalahti et al.*, 2006) and thus, competitor populations were not considered in this application.

Chlorinated solvent degradation was assumed to follow Monod kinetics (Fennell and Gossett, 1998; Lee et al., 2004; Christ and Abriola, 2006):

$$R_w^c = \begin{cases} \dfrac{C_w^c}{K_S^c + C_w^c} k_{\max}^c X_{FER}, c = Lactate \\ \dfrac{C_w^c k_{\max}^c X_{GEO}}{K_S^c + C_w^c} \times \dfrac{\left(C_w^H - C_w^{H-threshold-GEO}\right)}{K_S^{H-GEO} + \left(C_w^H - C_w^{H-threshold-GEO}\right)}, c = PCE, TCE \\ \dfrac{C_w^c k_{\max}^c X_{DHC}}{K_S^c I^c + C_w^c} \times \dfrac{\left(C_w^H - C_w^{H-threshold-DHC}\right)}{K_S^{H-DHC} + \left(C_w^H - C_w^{H-threshold-DHC}\right)}, c = DCE, VC \end{cases} \quad (6)$$

where model parameters are defined in Table 2. Note that an inhibition factor I^c is included for the 2nd dechlorinator population, X_{DHC}, to account for a decrease in dechlorinating activity due to the presence of PCE and competition among dechlorinating species for electron acceptors (Christ and Abriola, 2006):

$$I^c = \begin{cases} 1, & c = DCE, \\ 1 + \dfrac{C_w^{PCE}}{k_1^{PCE}} + \dfrac{C_w^{DCE}}{k_1^{DCE}}, & c = VC \end{cases} \quad (7)$$

Here, k_1^c is the inhibition coefficient due to the presence of c = PCE and *cis*-DCE. As shown in Eq. (7), PCE and *cis*-DCE inhibit degradation of VC, and hence the production of ethene. Equations (6) and (7) can be combined to form the bioreaction terms B_w^c in eq. (1a) and eq. (2)

according to: $B_w^{Lac} = -R_w^{Lac}$, $B_w^{PCE} = -R_w^{PCE}$, $B_w^{TCE} = R_w^{PCE} - R_w^{TCE}$, $B_w^{DCE} = R_w^{TCE} - R_w^{DCE}$, $B_w^{VC} = R_w^{DCE} - R_w^{VC}$, $B_w^{ETH} = R_w^{VC}$, and $B_w^{H_2} = F^{Lac} R_w^{Lac} - \sum_c F^c R_w^c$, where F^c is the stoichiometric production or use of hydrogen.

Microbial growth during each dechlorination step (dX/dt) was modeled using microorganism yield (Y^c) resulting from organohalide respiration, and the first-order endogenous decay rate (k_d) (Yu et al., 2005):

$$\frac{dX_{FER}}{dt} = Y^{Lac} R_w^{Lac} - k_d^{FER} X_{FER} \tag{8a}$$

$$\frac{dX_{GEO}}{dt} = Y^{PCE} R_w^{PCE} + Y^{TCE} R_w^{TCE} - k_d^{GEO} X_{GEO} \tag{8b}$$

$$\frac{dX_{DHC}}{dt} = Y^{DCE} R_w^{DCE} + Y^{VC} R_w^{VC} - k_d^{DHC} X_{DHC} \tag{8c}$$

where X_j is the attached active microbial cell concentration and k_d^j is the endogenous decay rate of population j. The DHB population was ignored due to the experimental observation that DHB did not colonize the column and hence had a nonexistent impact on dechlorination kinetics (Amos et al., 2009).

The set of equations (1) through (8) was implemented in MISER using a Galerkin finite element discretization method (Zienkiewicz and Taylor, 1991). The flow and transport equations in MISER, along with the constitutive relationships, have been verified by mass balance calculations and with analytical or other numerical solutions (Abriola et al., 1997, Rathfelder et al., 2000; Christ and Abriola, 2006). In the following sections, the experimental results of Amos et al. (2009) are used for model calibration and to evaluate the ability of the model to reproduce observed spatial and temporal trends related to the chloroethene reductive dechlorination and ethene formation.

2.2.4 Parameter Estimation

Application of any complex multi-phase, multi-constituent model requires the specification of a large number of system parameters and initial conditions. This section describes the approach used to estimate appropriate model parameters and any associated changes necessary to implement these in the simulator.

2.2.4.1 Initial hydrogeologic and biomass parameters

As described in Section 2.1 and shown in Figure 2, microbial dechlorination was not observed during the first 4 days of the experiment, and dechlorination that did occur from days 4 to 12 did not enhance PCE dissolution. One possible explanation for this lag is the organisms' acclimation period (Amos et al., 2009). To capture this effect in the model, the maximum utilization rates for dechlorination activity were set to zero for day 0 to day 4 and the initial *DHC* biomass concentrations measured in the two source zone ports ($x < 0.1$ m) were replaced with the biomass amounts measured in those ports at day 16 of the experiment; the first available side port sample data (see Figure 3 for biomass profiles). While some growth may have occurred during the first 4 days of the experiment, it was assumed to be negligible, consistent with this lack of dechlorination activity. Furthermore, initial numerical experiments suggested that the initial biomass concentrations (day 0) measured by Amos et al. (2009) were likely over-estimates of viable biomass, which was attributed to the introduction of PCE-containing NAPL in the source zone region.

Initial hydrogeologic parameters were obtained from direct experimental observations (Table 1). The lumped mass transfer coefficient during flow interruption was estimated to be 1.0×10^{-4} s^{-1} using a trial and error fitting process.

2.2.4.2 Biokinetic parameter estimates

Microbial kinetic parameters were not directly available from prior experimental work, and therefore, were estimated using inverse modeling. Estimates were needed for a total of 20 biological parameters, including the *maximum utilization rates* ($k^c_{\max}$), *half-saturation constants* (K^c_S) and *yield coefficients* (Y^c) for lactate fermentation and reductive dechlorination of PCE, TCE, *cis*-DCE, and VC (15 parameters), the *endogenous decay rate* (k_d) for three relevant microbial groups (FER, DHC, GEOSZ), and the *inhibition coefficients* (k^c_1) for PCE and *cis*-DCE (2 parameters), but not TCE since TCE did not accumulate. Initial values of these microbial kinetic parameters were derived from the literature (Table 2). Initial model calibration efforts revealed that the calibration process (inverse model convergence) proceeded more rapidly when the *maximum utilization rates* obtained from the literature were decreased by factors of four to 20 (Table 2). The need to adjust biokinetic parameters was expected given the variability of reported dechlorination rates for different consortia (Table 2). Note that all parameter adjustments fell within the range of values reported in the literature.

The large number of biokinetic parameters, coupled with the correlation between parameters and insensitivity of simulations to some parameters, resulted in an ill-defined matrix for inverse modeling as discussed below. Thus, the biokinetic calibration problem was simplified by identifying the eight most sensitive parameters, and subsequently focusing the inverse optimization effort on the parameters *maximum utilization rates* for PCE, TCE, *cis*-DCE, and VC (four parameters), biomass *yield* from PCE and *cis*-DCE degradation (two parameters), and *endogenous decay rates* of GEO and DHC (two parameters), which were considered adjustable parameters in Table 2. All other parameters were fixed at literature values, or related to other adjustable parameters as depicted in Table 2.

2.2.4.3 Parameter optimization and sensitivity analysis

PEST (Parameter ESTimation), a model-independent parameter estimator developed by Doherty (1994), was selected for parameter optimization based upon its extensive use and robust performance (e.g. Doherty, 2003; Gallagher and Doherty, 2006; Tonkin and Doherty, 2008). PEST employs a Levenberg-Marquardt nonlinear least squares fitting algorithm (Levenberg, 1944; Marquardt, 1963) to adjust input parameters to minimize the objective function $\phi = \sum_{i=1}^{m} \left(w_i r_i \right)^2$, where w_i and r_i express the weighting factor and the difference between model outcomes and the measurement for the *i*'th observation (error), respectively. Using the initial values shown in Table 2, the calibration process searched for the optimal set of biokinetic parameters that resulted in the smallest difference between the model-predicted and experimentally determined effluent concentrations of chlorinated ethenes. A total of 100 column effluent concentration observations for PCE, TCE, *cis*-DCE, VC, and ethene (20 observations for each of the chlorinated ethenes and ethene distributed from 5 to 50 days of column operation) were chosen for this calibration. To account for the large (approximately 10 times greater) *cis*-DCE concentrations relative to the other chlorinated ethenes, the *cis*-DCE concentrations were weighted by a 0.10 factor. This weighting ensured that the relative importance of each chlorinated ethene was similar. *Yield* values were constrained to the range reported in the literature (Table 2). Fitted parameters were log-transformed to approximate linearity, which facilitates optimization (Doherty, 1994).

Parameter optimization using PEST was distributed to multiple local network computers operated in a parallel configuration. The minimum number of model runs for each optimization iteration, the number required to calculate the Jacobian matrix (the matrix of the derivative of

observations with respect to parameters), was eight. The optimization process was assumed to be complete when three sequential iterations failed to decrease the value of the objective function.

Sensitivity of the 100 observations to the 20 biological model parameters, i.e., the *maximum utilization rates*, *yields*, and *half-saturation constants* (15 parameters), PCE and *cis*-DCE *inhibition constants* (2 parameters), and the *endogenous decay rates* of the FER, GEOSZ, and DHC (3 parameters) was examined using a Composite Sensitivity (CS) (Doherty, 1994) of each parameter p_i for each specific group containing n observations o_j:

$$CS_i = \frac{1}{n}\sqrt{\sum_j \left(\frac{\partial o_j}{\partial p_i} w_j\right)^2} \qquad (9)$$

where w_j is the weighting factor for observation o_j. In this study, 5 observation groups: PCE, TCE, *cis*-DCE, VC, and ethene effluent concentrations, each consisting of 20 observations, were considered. Additionally, the CS for all 20 parameters, based on a single group of all 100 observations, was used to evaluate the overall importance of each parameter.

3. Results and Discussion

3.1 Modeling Column Data

Comparisons of model simulations using the optimized parameter set (solid lines) with experimental measurements are shown in Figure 2. For the optimal fit shown in Figure 2 (Table 2 calibrated parameters), the model was run a total of 208 times. This comparison reveals that the calibrated effluent concentrations match the general trends of the experimental measurements well. Relative errors between experimental and simulated effluent concentrations (r_i) were typically less than 30% for each of the chlorinated ethenes and ethene except at late (>45 days) times (discussed below). As in the experiment, PCE dissolution and subsequent dechlorination

occurred with minimal TCE accumulation. Accumulation of *cis*-DCE and VC was observed beginning near day 12, presumably once the microbial populations had become acclimated. Comparison of simulated and experimental *cis*-DCE concentrations demonstrated close agreement across the observed concentration range (average r_i < 0.5%) and throughout most of the experimental period. However, comparison of simulated and observed VC and ethene effluent concentrations revealed significant deviation after day 45. Experimental VC and ethene concentrations were over-predicted immediately following the depletion of *cis*-DCE around day 46. Given that the predicted *cis*-DCE, VC and ethene concentrations at early times (< 40 days) showed good agreement with the experimental data (average r_i < 8%), there may be unidentified mechanisms (e.g., an unidentified biotic/abiotic process or loss) not captured by the model that resulted in lower dissolved phase VC and ethene concentrations. Total chloroethene-derived (includes ethene) mass balance in the experimental system was approximately 83%. Attempts to mimic this experimental behavior by reducing the overall chloroethene-derived mass in the initial system were unsuccessful, suggesting the process resulting in this behavior became more pronounced over time. One explanation is the formation of gas-filled pockets in the experimental column (e.g., Yang and McCarty, 2002; Amos et al., 2009). VC and ethene in the plume region could partition into these pockets, acting as a sink for these compounds and reducing their aqueous phase concentrations. Alternatively, recent work has suggested that back partitioning may influence degradation product partitioning among phases (Ramsburg et al., 2010a, 2010b). A lack of kinetic and equilibrium partitioning data for the chlorinated daughter products and ethene with the mixed NAPL prevent any effort to quantify the significance of this partitioning and the relatively short DNAPL source region (~10 cm) suggests any back partitioning is likely a secondary effect.

While the model described effluent concentration data quite well, a more revealing indicator of model performance is the ability of the calibrated model to predict the microbial activity measurements in the source zone and the plume region, data that were not used in the calibration process. A comparison of predicted and measured data from side port samples along the length of the column provides an independent assessment of the model's capability to simulate the reductive dechlorination process.

PCE, *cis*-DCE, and VC concentrations collected from side ports along the length of the column on days 16, 23 and 42 were compared to corresponding simulated concentrations in Figure 4. At day 16 (Figure 4a), the model predicted *cis*-DCE and VC concentrations along the length of the column (r_i typically less than 10% for *cis*-DCE and 20% for VC); however, PCE concentrations were significantly under-predicted (r_i ~ 70%). This could indicate greater simulated microbial activity in the source zone at day 16 or that the Sherwood number employed in the model under-estimated the mass transfer rate, leading to the under-estimation of dissolved-phase PCE concentrations in the source region (x < 0.15m). No attempt was made to fit the mass transfer rate since dissolution kinetics are well established (Powers et al., 1994). In the day 23 comparison (Figure 4b), PCE was still present in the source zone and significant amounts of *cis*-DCE and VC had been formed in the experimental system. Model simulations provided accurate predictions of experimental observations of *cis*-DCE (r_i typically less than 10%) and predictions within an order-of-magnitude for VC (r_i typically less than 70%), but again tend to under-estimate the PCE concentration in the source region. When compared to day 42 experimental results (Figure 4c), the model captured the general behavior of the *cis*-DCE and VC concentrations along the length of the column (average $r_{cis\text{-}DCE}$ < 5% and r_{VC} typically less than 60%). The variability in the *cis*-DCE measurements along the length of the column is likely due

to the spatial variability in PCE dissolution as the PCE was depleted from the source zone at later times. Given that the model is one-dimensional (1-D), it is not capable of capturing small scale nonuniformity in domain conditions that emerge over time, although it does capture the general increase and plateau of *cis*-DCE and VC concentrations.

In addition to chloroethene-derived concentrations, model predictions of microbial growth were evaluated, a comparison that is generally absent in the literature. Unattached ("planktonic") aqueous phase microbial cells were measured from the side ports during column operation (Figure 5). The model assumes a total active biomass consisting of both attached and unattached cells. To facilitate comparisons between experimental biomass measurements (unattached) and the model predictions (total), the ratio between total and unattached biomass was estimated at 16, 23, and 42 days (Table 3). This ratio was assumed to be a constant in the source zone ($x < 0.15$ m) and the plume region (0.15 m $< x < 0.60$ m) at each sampling time, and was adjusted within the experimental range given by the initial (day 0) and final (day 42) measurements to give the best visual fit to the *GEO* and *DHC* spatial distributions along the column. Figure 5 depicts experimental and simulated unattached *GEO* and *DHC* biomass data. The simulated biomass profiles scaled to reflect only the unattached biomass are in agreement with experimental measurements at most of the side-ports on day 16 (median r_{GEO} = 10.5% and r_{DHC} = 7.0%). Although by day 23 and day 42 the model over-estimated the DHC biomass in the plume region, model predictions are still within approximately one order-of-magnitude of experimental observations (Figure 5b, c; median r_{GEO} = 20% and r_{DHC} = 170% at day 23 and r_{GEO} = 35% and r_{DHC} = 112% at day 42). Note that fitting the total to unattached biomass ratio served to scale (i.e, to adjust the simulated curve up and down) the spatial distribution, but did

not alter the spatial trends in biomass along the column length. Thus, the mathematical model served as a good predictor for the observed microbial growth patterns.

3.2 Sensitivity Analysis

3.2.1 Composite sensitivity of microbial kinetics

Based on the results presented in the previous section, the calibrated model was used to assess the sensitivity of reductive dechlorination activity to model parameters by identifying the relative importance of each of the kinetic parameters (Table 2) using the CS. Figure 6 depicts the CS for each parameter for each group of concentration measurements. Figures 6a and 6b indicate the first two reductive dechlorination steps from PCE via TCE to *cis*-DCE are most sensitive to the PCE *maximum utilization rate* ($k_{\max}^{PCE}$). As anticipated, *cis*-DCE predictions are most sensitive to $k_{\max}^{PCE}$, indicating the accumulation of *cis*-DCE was influenced by the degradation of the higher chlorinated contaminants more so than the rate of *cis*-DCE dechlorination (low CS for $k_{max}{}^{DCE}$). The *cis*-DCE-to-VC dechlorination step appears to be nearly as sensitive to the growth of the GEO population, as indicated by the high CS for Y_{PCE} (Figure 6c). The degradation of *cis*-DCE ($k_{\max}^{DCE}$), as well as the growth of the DHC population (Y^{DCE}, k_d^{DHC}), controlled the second phase of the dechlorination process (i.e., *cis*-DCE to ethene, Figure 6d and 6e). Interestingly, Figure 6f shows that the overall model results are most sensitive to the *cis*-DCE *maximum utilization rate* ($k_{\max}^{DCE}$) and *yield* of *cis*-DCE (Y^{DCE}), followed by the similar parameters governing PCE degradation. This finding suggests that PCE and *cis*-DCE degradation are the key steps in the sequential dechlorination process. Apparently, once dechlorination from *cis*-DCE to VC occurs, the final dechlorination step to ethene is not limiting in this system. Sensitivities of kinetic parameters associated with lactate fermentation ($k_{\max}^{Lac}$,

K_S^{Lac}, k_d^{FER}) were not significant in this modeling application due to the consistent delivery of sufficient electron donor to fully support reductive dechlorination reactions. These results are consistent with earlier findings of Kouznetsova et al. (2010), who showed that dechlorination in a batch system was most sensitive to ($k_{\max}^{DCE}$) and (Y^{DCE}). However, their system did not consider the PCE-to-TCE dechlorination step and did not include NAPL dissolution.

3.2.2 Inhibition

Although the above sensitivity analysis indicated that model predictions were not sensitive to the *cis*-DCE inhibition coefficient (k_1^{DCE}) for these experimental conditions, inhibitory effects of polychlorinated ethenes are often cited as a reason for incomplete dechlorination to ethene (e.g., Haest et al., 2010; Sabalowsky and Semprini, 2010a, 2010b; Amos et al., 2009). The calibrated model allows for a more detailed analysis to assess the influence of inhibition on the complete dechlorination of *cis*-DCE and VC to ethene. Figure 7 depicts the simulated accumulation of *cis*-DCE, VC, and ethene in the column effluent using a no-inhibition scenario and the inhibition coefficients listed in Table 2. In the former case, total ethene production increased ten-fold and total *cis*-DCE and VC formation were reduced by 25% and 20%, respectively. Thus, while the model results were relatively insensitive to the magnitude of the inhibition coefficient, neglecting inhibition could lead to substantial underestimation of the accumulation of VC and overestimation of the complete conversion to ethene.

3.2.3 Column residence time

The experimental results of Amos et al. (2009) suggest that the column residence time was insufficient for complete dechlorination, and thus, a series of numerical studies was performed to examine the influence of residence time (i.e., column length and aqueous phase

flow rate) on simulation results. In these numerical studies, the column length was first halved, and then doubled, relative to the initial column length (60 cm), while all other parameters were kept constant (see Tables 1 and 2). Simulation results for the shortened column resulted in a decrease in the total production of *cis*-DCE, VC, and ethene by 19%, 53%, and 73%, respectively (Figure 8). As expected, the reduced column length resulted in a residence time that was insufficient for complete PCE conversion to *cis*-DCE. When the column length was doubled, less *cis*-DCE accumulated, while VC and ethene production increased significantly. The 42% reduction in *cis*-DCE production (up to day 55) in the longer column indicated that the original column length was insufficient to achieve complete dechlorination to ethene. In the longer column with increased residence time, the microbial consortium was predicted to dechlorinate *cis*-DCE more effectively, resulting in a 4-fold and a 9-fold increase in VC and ethene production, respectively (Figure 8).

A simpler experimental method for modifying residence time in the column is to change the aqueous phase flow rate. However, changing the aqueous phase flow rate not only affects column residence time, but also impacts the rate of PCE mass transfer from the NAPL to the aqueous phase (see Eq.5). In this set of simulations, the aqueous phase flow rate was first halved and then doubled for comparison with the original simulation conditions. As expected, maximum PCE discharge (μg/min) during the initial 4 days was linearly proportional to the flow rate due to the fact that the equilibrium aqueous phase PCE concentration was reached in all three cases (Figure 9). When the flow rate was doubled, *cis*-DCE and VC reached higher maximum discharge levels after the flow interruption (dashed vertical lines in Figure 9), but were also depleted faster (Figure 9) than in the base case simulation, resulting in less total mass recovered (Figure 10). Ethene production occurred earlier in the doubled flow rate simulation,

but decreased earlier due to less VC available. In the reduced flow rate simulation, VC degradation was inhibited by the elevated *cis*-DCE concentrations (see eq. 7, k_I^{DCE} = 0.52.4 μg/L, Table 2) resulting in minimal ethene production by the end of the simulation (Figure 10). Thus, despite the longer residence time, microbial inhibition resulting from elevated levels of cis-DCE prevented complete dechlorination to ethene.

Interestingly, the model predictions indicate that the total mass of chlorinated ethenes and ethene recovered in the column effluent increases in proportion to the flow rate due to the increase in PCE dissolution (Figure 11). At the high flow rate, more PCE dissolved into the aqueous phase and was recovered in the effluent, leading to a higher total mass recovery. However, less PCE was dechlorinated to *cis*-DCE (45% less than baseline), VC (39% less), and ethene (73% less). Although 91% and 169% more *cis*-DCE and VC, respectively, were produced under the slow flow condition, PCE dissolution was reduced, resulting in greater PCE mass remaining in the NAPL. Additionally, 38% less ethene was produced in the low flow column due to inhibition of VC reductive dechlorination due to the high *cis*-DCE concentrations. These findings indicate that residence time in the bioactive zone is a key factor determining detoxification (i.e., ethene formation). The refined model will be useful to optimize the design of source zone bioremediation in order to achieve treatment objectives, whether that means removal of contaminant mass from the system as rapidly as possible, or complete dechlorination to non-toxic ethene, or both.

4. Conclusions

A multiphase compositional simulator was designed to accurately represent the sequential reductive dechlorination process converting PCE to ethene by a microbial consortium containing *Geobacter* and *Dehalococcoides* populations under dynamic conditions. The dechlorination

process resulted in enhanced dissolution of PCE from a source zone containing a mixed NAPL at residual saturation. The model was calibrated to effluent chlorinated ethenes and ethene concentrations measured during a bioenhanced dissolution column experiment by optimizing the eight most sensitive microbial kinetic parameters using a best-fit calibration process. Model simulations generally captured measured effluent concentrations of all five chlorinated ethene constituents (predicted to experimental relative errors less than 30%). Simulated VC and ethene concentrations were higher than observed values, possibly due to gas evolution and gas phase partitioning, which were not considered in the model. Following calibration, model predictions were compared to concentrations of chlorinated ethenes and biomass measured in side-port samples collected at three different times. This novel validation methodology demonstrated model accuracy and applicability using a single set of experimental results. This level of model validation has not been conducted for any dechlorinating consortium to date, and thus, the present work provides a unique opportunity to verify the conceptual models of microbial kinetics commonly employed in dechlorination simulators.

Using the calibrated model, a detailed sensitivity analysis was performed to investigate the relative influence of 20 microbial kinetic parameters on the overall model performance. The composite sensitivity assessment suggested that degradation of PCE and *cis*-DCE are key processes controlling complete dechlorination to ethene. A step-by-step evaluation of dechlorination kinetics revealed that the higher chlorinated contaminants (PCE and TCE) were most sensitive to the PCE *maximum utilization rate*, while the lesser chlorinated contaminants (*cis*-DCE and VC) were most sensitive to *cis*-DCE dechlorination and DHC growth kinetics. Simulations that neglected inhibition resulted in a 10-fold increase in ethene production, demonstrating the importance of inhibitory factors on bioactivity. Altering the column length or

flow rate to increase or decrease residence time also indicated that complete dechlorination to ethene was influenced by a balance between sufficient residence time to achieve complete dechlorination without allowing for accumulation of *cis*-DCE, which inhibits the final dechlorination step. The verified model may be used to investigate bioenhanced dissolution in field settings, and as a guide to design biostimulation and bioaugmentation strategies for source zone treatment in conjunction with, or following, aggressive mass removal.

Acknowledgements

This research was supported by the Strategic Environmental Research and Development Program (SERDP) under contract W912HQ-04-0006 (Project ER-1293) and contract W91HQ-08-C-0003 (Project ER-1612). This content of this manuscript has not been subject to agency review and does not necessarily represent the view of the agency sponsor.

Prepared by LLNL under Contract DE-AC52-07NA27344.

References

Abriola, L.M., Lang, J.R., Rathfelder, K. (1997) *Michigan soil–vapor extraction remediation (MISER) model – A computer program to model bioventing of organic chemicals in unsaturated geological material*. U.S. Environmental Protection Agency, EPA 600-R-97-099.

Adamson, D.T., McDade, J.M., Hughes, J.B. (2003) Inoculation of a DNAPL source zone to initiate reductive dechlorination of PCE. *Environ. Sci. Technol*, 37, 2525-2533.

Amos, B.K., Christ, J.A., Abriola, L.A., Pennel, K.D., Löffler, F.E. (2007) Experimental evaluation and mathematical modeling of microbially enhanced tetrachloroethene (PCE) dissolution. *Environ. Sci. Techno*l, 41, 963-970.

Amos, B.K., Suchomel, E.J., Pennell, K.D., Löffler, F.E. (2008) Microbial activity and distribution during enhanced contaminant dissolution from a NAPL source zone. *Water Res., 42,* 2963-2974.

Amos, B.K., Suchomel, E.J., Pennell, K.D., Löffler, F.E. (2009) Spatial and temporal distributions of Geobacter lovleyi and Dehalococcoides spp. during bioenhanced PCE-NAPL dissolution. *Environ. Sci. Technol*, 43, 1977-1985.

Bagley, D.M. (1998) Systematic approach for modeling tetrachloroethene biodegradation. *J. Environ. Eng*., 124, 1076-1086.

Battisstelli, A. (2004) Modeling biodegradation of organic contaminants under multiphase conditions with TMVOCBio. *Vadose Zone J*, 3, 875–883.

Becker, J.G. (2006) A modeling study and implications of competition between Dehalococcoides ethenogenes and other tetrachloroethene-respiring bacteria. *Environ. Sci. Technol*., 40, 4473–4480.

Becker, J.G, Seagren E.A. (2009) Modeling the effects of microbial compeitition and hydrodynamics on the dissolution and detroxification of dense nonaqueous phase liquid contaminants. *Environ. Sci. Technol*., 43, 870-877.

Carr, C.S., Garg, S., Hughes, J.B. (2000) Effect of dechlorinating bacteria on the longevity and composition of PCE-containing nonaqueous phase liquids under equilibrium dissolution conditions. *Environ. Sci. Technol*., 34, 1088–1094.

Christ, J.A., Ramsburg, C.A., Löffler, F.E., Pennell, K.D., Abriola, L.M. (2005) Coupling aggressive mass removal with microbial reductive dechlorination for remediation of DNAPL source zones – a review and assessment. *Environ. Health Perspect*., 113, 465–477.

Christ, J.A., Abriola, L.M. (2006) Modeling metabolic reductive dechlorination in dense non-aqueous phase liquid source zones. *Adv. Water Resour*., doi:10.1016/j.advwatres.2006.05.024.

Chambon, J.C., Broholm, M.M., Binning, P.J., Bjerg, P.L. (2010) Modeling multi-component transport and enhanced anaerobic dechlorination processes in a single fracture-clay matrix system. *J. Contam. Hyd*., 112, 77-90.

Chu, M., Kitanidis, P.K., McCarty, P. (2003) Effects of biomass accumulation on microbially enhanced dissolution of a PCE pool: a numerical simulation. *J. Contam. Hydrol*., 65, 79-100.

Chu, M., Kitanidis, P.K., McCarty, P.L. (2004) Possible factors controlling the effectiveness of bioenhanced dissolution of nonaqueous phase tetrachloroethene. *Adv. Water Resour*., 27, 601–615.

Chu, M., Kitanidis, P.K., McCarty, P.L. (2006) Inhibition-related limitation to biologically enhanced dissolution of chlorinated solvents. *Proceedings of the Fifth International Conference on Remediation of Chlorinated and Recalcitrant Compounds*, Monterey, CA, May 22-25, 2006; Curran Associates: Red Hook, NY, 2006; Abstract B-24.

Clapp, L.W., Semmens, M.J., Novak, P.J., Hozalski, R.M. (2004) Model for in situ perchloroethene dechlorination via membrane delivered hydrogen. *J. Environ. Eng.*, 130, 1367 – 1381.

Clement, T.P., Gautam, T.R., Lee, K.K., Truex, M.J., Davis, G.B. (2004) Modeling of DNAPL-dissolution, rate-limited sorption and biodegradation reactions in groundwater systems. *Bioremed. J.,* 8, 47–64.

Cope, N, Hughes, J.B. (2001) Biologically-enhanced removal of PCE from NAPL source zones. *Environ. Sci. Technol*., 35, 2014-2021.

Da Silva, M.L., Daprato, R.C., Gomez, D.E., Hughes, J.B., Ward, C.H., Alvarez, P.J. (2006) Comparison of bioaugmentation and biostimulation for the enhancement of dense nonaqueous phase liquid source zone bioremediation. *Water Environ. Res*., 78, 2456–2465.

Delshad, M., Pope, G.A., Sepernoori, K. (1996) A compositional simulator for modeling surfactant enhanced aquifer remediation. *J Contam. Hydrol*., 23, 303–327.

Doherty, J. (1994) *Model-independent parameter estimation*. 5th Ed. Watermark Numerical Computing. Brisbane, Australia, 336 p.

Doherty, J. (2003) Groundwater model calibration using pilot points and regularization. *Ground Water,* 41, 170-177.

Driscoll, F.G. (1986) *Groundwater and Wells*. Johnson Filtration Systems, Inc., St. Paul, MN, 2nd ed., 1089 pp.

Fennell, D.E., Gossett, J.M. (1998) Modeling the production of and competition for hydrogen in a dechlorinating culture. *Environ. Sci. Technol*., 32, 2450-2460.

Gallagher, M.R., Doherty, J. (2006) Parameter estimation and uncertainty analysis for a watershed model. *Environ. Model. Software*, 22, 1000-1020.

Glover, K.C., Munakata-Marr, J., Illangasekare, T.H. (2007) Biologically enhanced mass transfer of tetrachloroethene from DNAPL source zones: experimental evaluation and influence of pool morphology. *Environ. Sci. Technol*., 41, 1384-1389.

Hammond, G.E., Valocchi, A.J., Lichtner, P.C. (2005) Application of Jacobian-free Newton-Krylov with physics-based preconditioning to biogeochemical transport. *Adv. Water Resour*., 28, 359-376.

Haest, P.J., Springael, D., Smolders, E. (2010) Dechlorination kinetics of TCE at toxic TCE concentrations: Assessment of different models. *Water Res*., 44, 331-339.

Huang, D., Becker, J.G. (2009) Determination of intrinsic monod kinetic parameters for two heterotrophic tetrachloroethene (PCE)-respiring strains and insight into their application. *Water Res.* 104, 301-311.

Huang D., Becker, J.G. (2011) Dehalorespiration model that incorporates the self-inhibition and biomass inactivation effects of high tetrachloroethene concentrations. *Environ. Sci. Technol.*, 45, 1093-1099.

Imhoff, P.T., Jaffe, P.R., Pinder, G.F. (1994) An experimental-study of complete dissolution of a nonaqueous phase liquid in saturated porous-media. *Water Resour. Res*., 30, 307-320.

Kouznetsova, I., Mao, X., Robinson C., Barry D.A., Gerhard J.I., McCarty P.L. (2010) Biological reduction of chlorinated solvents: Batch-scale geochemical modeling. *Adv. Water Resour*., 33, 969-986.

Lee, I.S., Bae, J.H., Yang, Y., McCarty, P.L. (2004) Simulated and experimental evaluation of factors affecting the rate and extent of reductive dehalogenation of chloroethenes with glucose. *J. Contam. Hydrol*., 74, 313-331.

Levenberg, K. (1944) A Method for the Solution of Certain Non-Linear Problems in Least Squares. *Quarterly Applied Math.*, 2, 164–168.

Marquardt, D. (1963) An Algorithm for Least-Squares Estimation of Nonlinear Parameters. *SIAM J. Applied Math.*, 11, 431–441.

Miller, C.T., Poirier-McNeill, M.M., Mayer, A.S. (1990) Dissolution of trapper nonaqueous phase liquids: Mass transfer characteristics. *Water Resour. Res*., 26, 2783-2796.

Mravik, S.C., Sillan, R.K., Wood, A.L., Sewell, G.W. (2003) Field evaluation of the solvent extraction residual biotreatment technology. *Environ. Sci. Technol*., 37, 5040–5049.

Philips, J., Springael, D., Smolders, E. (2011) A three-layer diffusion-cell to examine bio-enhanced dissolution of chloroethene dense non-aqueous phase liquid. *Chemosphere*, 83, 991-996.

Powers, S.E., Abriola, L.M., Weber Jr, W.J. (1992) An experimental investigation of nonaqueous phase liquid dissolution in saturated subsurface systems: steady state mass transfer rates. *Water Resour. Res*., 28, 2691-2705.

Powers, S.E., Abriola, L.M., Weber Jr, W.J. (1994) An experimental investigation of nonaqueous phase liquid dissolution in saturated subsurface systems: transient mass transfer rates. *Water Resour. Res*., 30, 321-332.

Ramsburg, C.A., Abriola, L.M., Pennell, K.D., Löffler, F.E., Gamache, M., Amos, B.K., Petrovskis, E.A. (2004) Stimulated microbial reductive dechlorination following surfactant treatment at the Bachman Road site. *Environ Sci Technol*., 38, 5902–5914.

Ramsburg, C.A., Thornton, C.E., Christ, J.A. (2010) Degradation product partitioning in source zones containing chlorinated ehtene dense non-aqueous-phase liquid. *Environ. Sci. Technol*., 44, 9105 – 9111.

Rathfelder, K.M., Abriola, L.M., Singletary, M.A., Pennell, K.D. (2000) The influence of interfacial tension reduction on organic liquid migration: numerical and experimental comparisons. In: *Proc ModelCARE 99: calibration and reliability in groundwater modelling, coping with uncertainty*, Zurich, Switzerland.

Sabalowsky, A.R., Semprini, L. (2010a) Trichloroethene and cis-1,2-dichloroethene concentration-dependent toxicity model simulates anaerobic dechlorination at high concentrations: 1. Batch-fed reactors. *Biotechnol. Bioeng*., 107, 529-539.

Sabalowsky, A.R., Semprini, L. (2010b) Trichloroethene and cis-1,2-dichloroethene concentration-dependent toxicity model simulates anaerobic dechlorination at high concentrations: 2. Continuous flow and attached growth reactors. *Biotechnol. Bioeng*., 107, 529-539.

Schaefer, C.E., Towne, R.M., Vainberg, S., McCray, J.E., Steffan, R.J. (2010) Bioaugmentation for treatment of dense non-aqueous phase liquid in fractured sandstone blocks. *Env Sci Technol*., 44, 4958 – 4964.

Schwarzenbach, R.P., Gwchwend, P.M., Imboden, D.M. (2003) *Environmental Organic Chemistry*. New York, NY, Wiley.

Seeliger, S., Janssen, P.H., Schink, B. (2002) Energetics and kinetics of lactate fermentation to acetate and propionate via methylmalonyl-CoA or acrylyl-CoA. *FEMS Microbiology Letters*, 211, 65-70.

Sleep, B.E., Seepersad, D.J., Mo, K., Heidorn, C.M., Hrapovic, L, Morrill, PL, McMaster, M.L, Hood, ED, Lebron, C, Sherwood LB, Major, DW, Edwards, EA. (2006) Biological enhancement of tetrachloroethene dissolution and associated microbial community changes. *Environ. Sci. Technol*., 40, 3623-3633.

Suchomel, E.J., Ramsburg, C.A., Pennell, K.D. (2007) Evaluation of trichloroethene recovery processes in heterogeneous aquifer cells flushed with biodegradable surfactants. *J. Contam. Hydrol*., 93, 195–214.

Tonkin, M., Doherty, J. (2008) Calibration-constrained Monte Carlo analysis of highly-parameterized models using subspace techniques. *Water Resour. Res*., 45, W00B10, doi:10.1029/2007WR006678.

Widdowson, M.A. (2004) Modeling natural attenuation of chlorinated ethenes under spatially varying redox conditions. *Biodegradation*, 15, 435-451.

Willis, M., Shoemaker, C. (2000) Engineered PCE dechlorination incorporating competitive biokinetics: optimization and transport modeling. In: Wickramanayake GB, Gavaskar AR, Alleman BC, Magar VS, editors. *Bioremediation and phytoremediation of chlorinated and recalcitrant compounds*. Columbus, OH: Battelle Press, 311-318.

Santos, A., Barros, P.H.L. (2010) Multiple particle Retention Mechanisms during Filtration in Porous Media. *Environ. Sci. Technol*., 44, 2515-2521.

Yang, Y., McCarty, P.L. (2000) Biologically enhanced dissolution of tetrachloroethene DNAPL. *Environ. Sci. Technol*., 34, 2979-2984.

Yang, Y., McCarty, P.L. (2002) Comparison between donor substrates for biologically enhanced tetrachloroethene DNAPL dissolution. *Environ. Sci. Technol*., 36, 3400-3404.

Yu, S., Semprini, L. (2004) Kinetics and modeling of reductive dechlorination at high PCE and TCE concentrations. *Biotechnol. Bioeng*., 88, 451-464.

Yu, S., Dolan, M.E., Semprini, L. (2005) Kinetics and inhibition of reductive dechlorination of chlorinated ethylenes by two different mixed cultures. *Environ. Sci. Technol*., 39, 195-205.

Zienkiewicz, O.C., Taylor, R.L. (1991) *The Finite Element Method*, McGraw-Hill, London, 1991.

Table 1. Physical Column Experimental Parameters

Parameters	**Value**
Porosity, -	0.374[a]
Median grain size d_{50}, mm	0.32[a]
Uniformity index (d_{60}/ d_{10}), -	1.86[b]
Bulk soil density, g/cm^3	2.03[c]
Intrinsic permeability, darcy	42.0[a]
Dispersivity, m	0.01[d]
PCE-Hexadecane (HD) mole ratio	0.25/0.75
PCE/HD-NAPL density, g/cm^3	0.86[a]
Bottom water flux, mL/min	0.25, 0, 0.1[e]
Column length, cm	60
Column diameter, cm	4.8
Total pore volume, cm^3	407[c]
Source zone position & saturation	0-10 cm[f] & 0.21[g]
Transition zone position & saturation	10-15 cm[f] & 0.21 to 0.08[g]

[a] Estimated from Suchomel et al., 2007.
[b] Estimated from Santos and Barros, 2010.
[c] Estimated from Amos et al., 2009.
[d] Assumed.
[e] Initial flow 0.25mL/min; flow interruption at 19th day for 22 hours; 0.1 mL/min after 24th day.
[f] Visual observation
[g] Total NAPL volume was 14 mL based on Amos et al., 2009.

Table 2. Initial and calibrated model coefficients for dechlorination used in simulations

Parameters	Type	Literature[1]	Initial[2]	Calibrated
Maximum utilization rate $k^c_{\max}$ *(μmol/mg-day)*				
Lactate	Fixed	206	206	-
PCE	Adjustable	1.4 - 117	14	94
TCE	Adjustable	2.4 - 366	24	80
DCE	Adjustable	1.7 – 48	18	30
VC	Adjustable	2.6 – 48	3.2	6.9
Yield Y^c *(g cell/mol substrate)*[3]				
Lactate	Fixed	1.5-6.3	3.9	-
PCE	Adjustable	7.54-22.6	15.1	17.9
TCE	Tied	$=Y^{PCE}$	15.1	17.9
DCE	Adjustable	5.89-8.25	7.07	5.89
VC	Tied	$=Y^{DCE}$	7.07	5.89
Half-saturation constant K^c_S *(μM)*				
Lactate	Fixed	2.5	2.5	-
PCE	Fixed	0.11 – 2.8	0.54	-
TCE	Fixed	0.54 – 1.5	0.54	-
DCE	Fixed	0.54 – 3.3	0.54	-
VC	Fixed	0.54 - 360	0.54	-
Inhibition coefficients k^c_1 *(μM)*[4]				
PCE	Fixed	$=K_S^{PCE}$	0.54	-
DCE	Fixed	$=K_S^{VC}$	0.54	-
Microbe decay rate k_d *(1/day)*				
Fermentor	Fixed	0.050	0.050	-
Geobacter	Adjustable	0.050	0.050	0.063
Dehalococcoides	Adjustable	0.050	0.050	0.048

[1] Literature values for the Maximum utilization rate and half saturation constant were taken from Clapp et al. (2004) and Lee et al. (2004); Yield for lactate and chlorinated ethenes are taken from Seeliger et al.(2002) and Amos et al. (2009).

[2] Initial values for calibration process are estimated based on the literature.

[3] Y^{TCE} and Y^{VC} are tied to Y^{PCE} and Y^{DCE} respectively, and are not included in the optimization process.

[4] Inhibition coefficients are tied to the corresponding half-saturation constant as discussed in Christ and Abriola (2006).

Table 3. Total/unattached ratio of biomass in column

	Source zone	Plume zone
Initial[a]		
Geobacter	20	20
Dehalococcoides	20	20
Day 16[b]		
Geobacter	20	10
Dehalococcoides	20	10
Day 23[b]		
Geobacter	20	10
Dehalococcoides	10	5
Day 42[b]		
Geobacter	20	2
Dehalococcoides	10	2
Final[a]		
Geobacter	4 - 20	1
Dehalococcoides	10	1.25

[a] Ratio based on experimental measurements prior to column operation and at completion of the experiment.
[b] Ratio based on best-fit to side port samples of biomass concentrations.

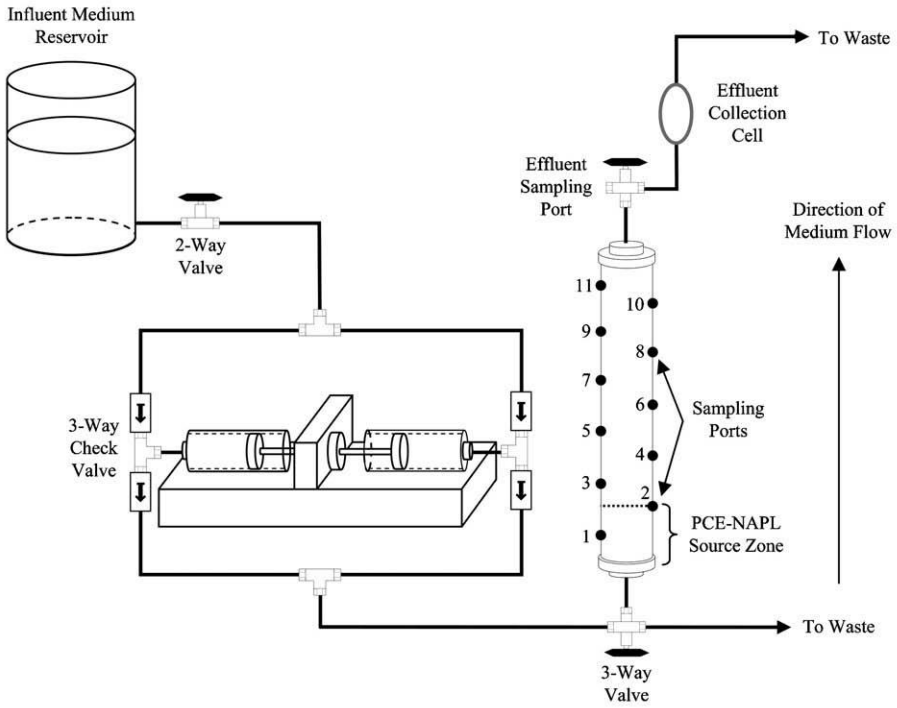

Figure 1. Experimental column diagram adapted from Amos et al. (2008)

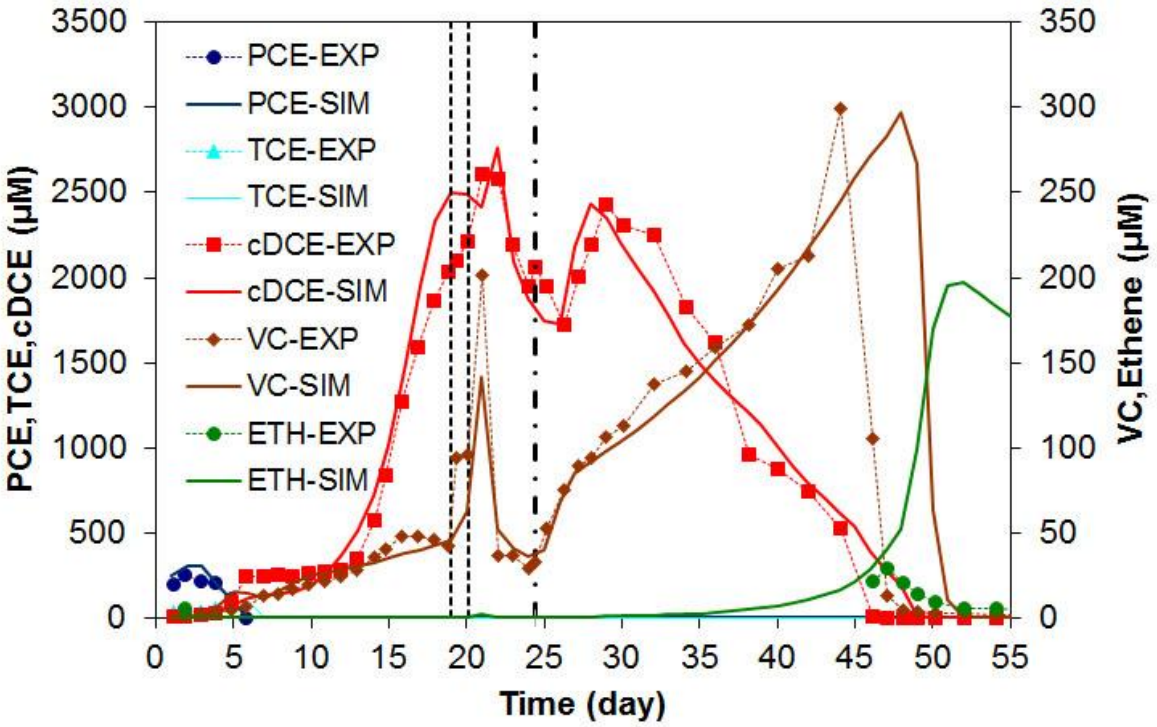

Figure 2. Comparison between simulated (solid line) and experimental (dashed line with marker) organic effluent concentrations. Flow was interrupted between two vertical dashed lines and was decreased from 0.25 mL/min to 0.1 mL/min after vertical dash-dot line on 24th day.

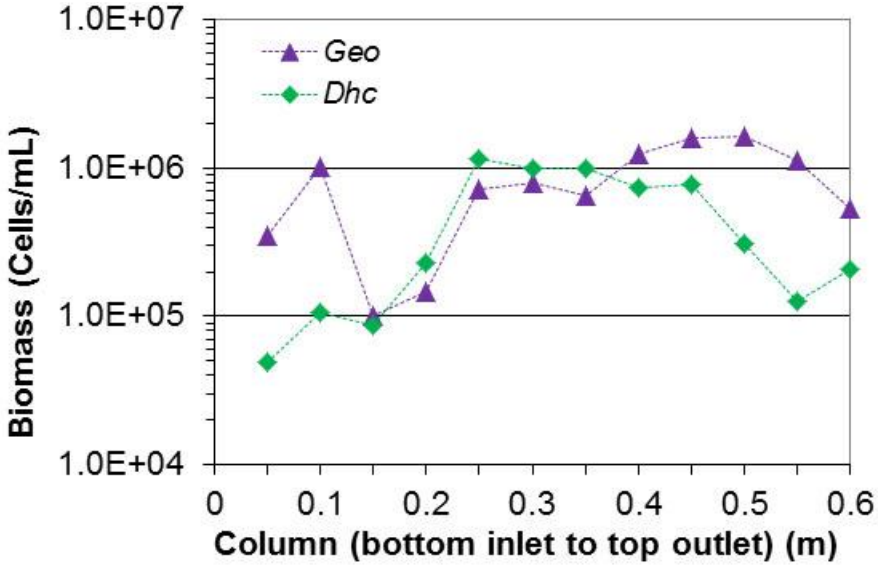

Figure 3. Side-port samples of initial *Geobacter* (GEO) and *Dehalococcoides* (DHC) concentrations along the column. The initial values of DHC at port 1 and 2 (5 and 10 cm – first two data points) are replaced by those at day 16.

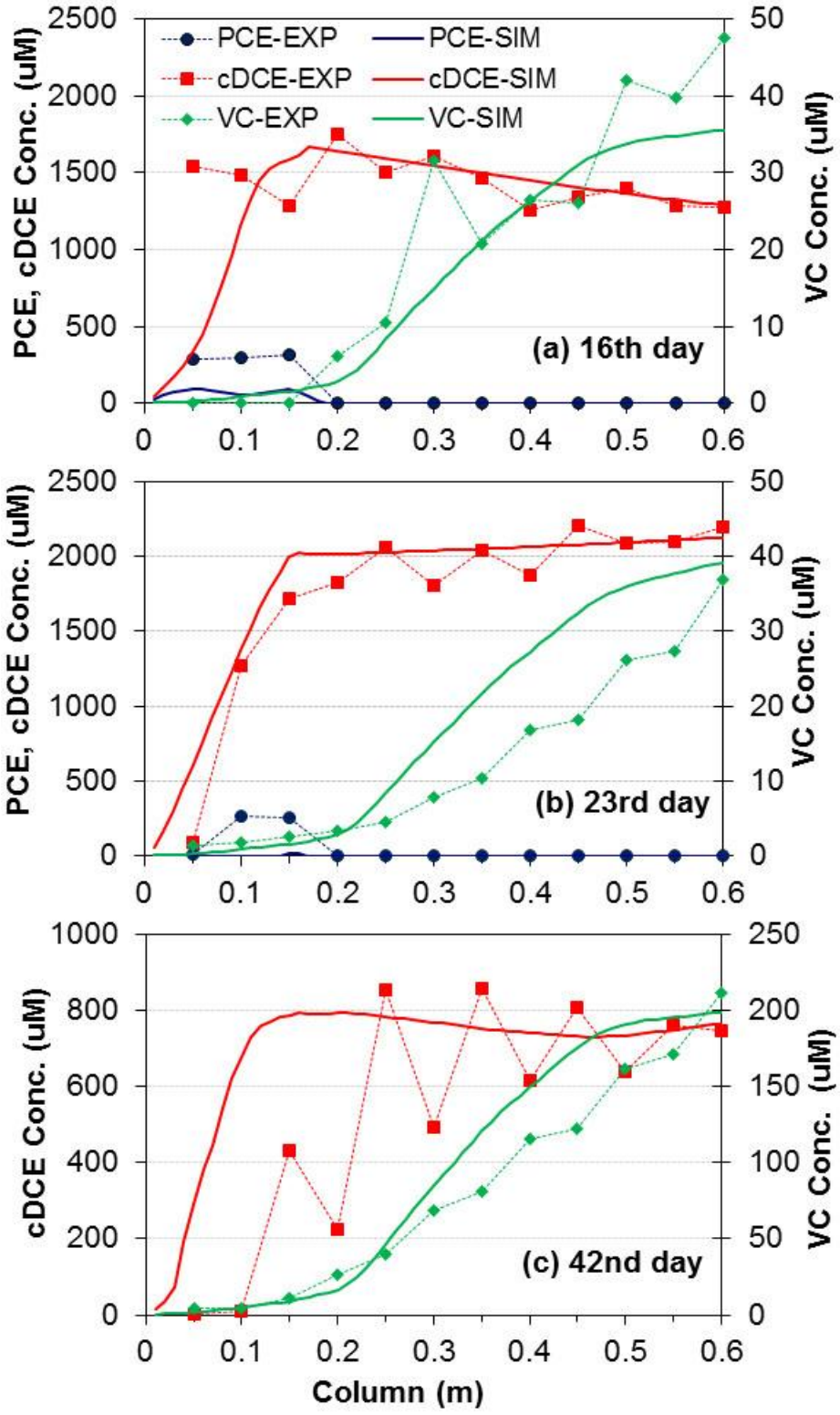

Figure 4. Comparison of predicted (solid line) and experimental (symbols) PCE, *cis*-DCE, and VC concentrations from the side-port samples along the column at (a) 16 days, (b) 23 days, and (c) 42 days.

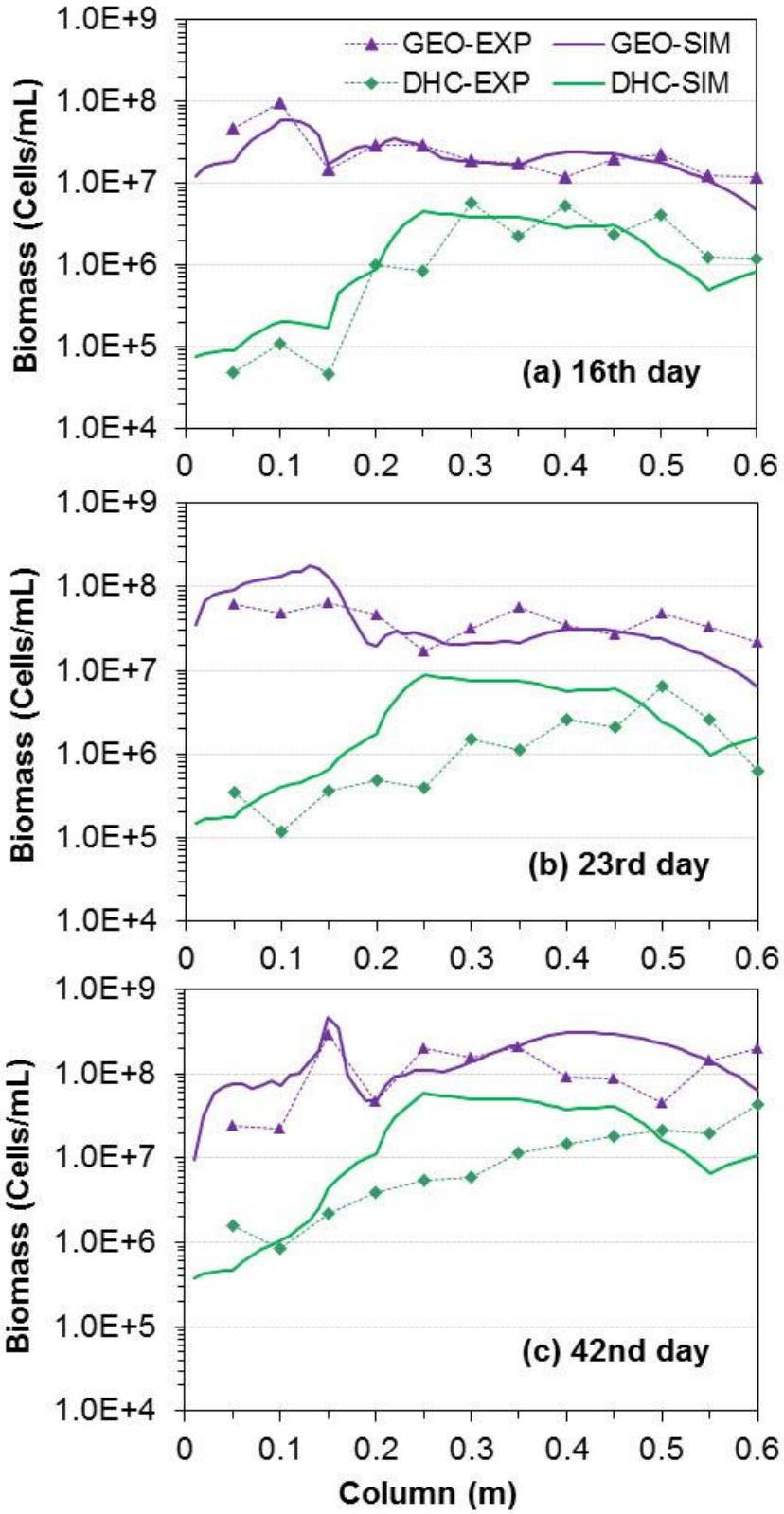

Figure 5. Comparison of predicted (solid line) and experimental (symbols) planktonic biomass (*Geobacter* (GEO) and *Dehalococcoides* (DHC)) with the side-port samples along the column at (a) 16 days, (b) 23 days, and (c) 42 days.

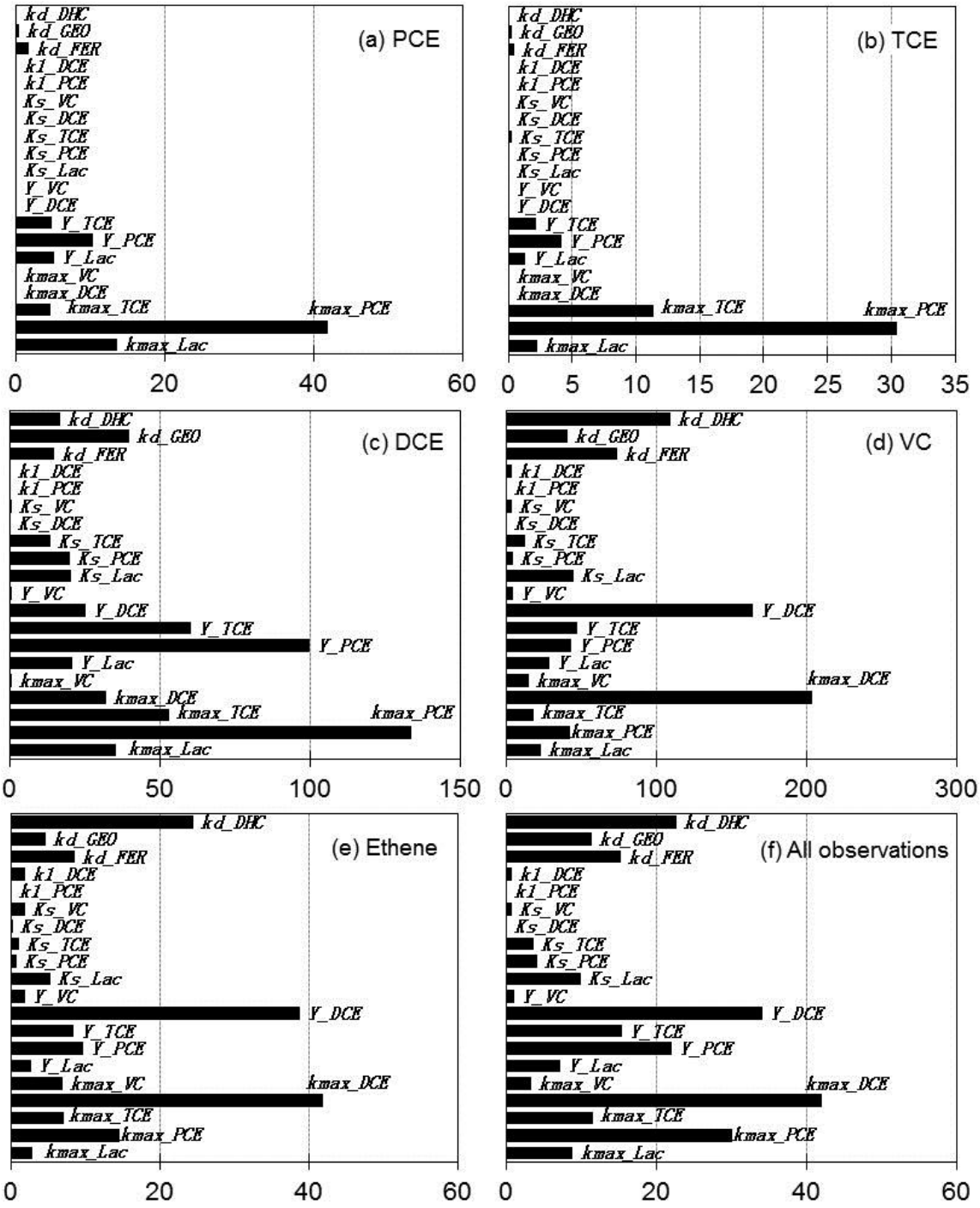

Figure 6. Composite sensitivity (CS) of kinetic parameters (see Table 2 for kinetic parameters) to (a) PCE, (b) TCE, (c) *cis*-DCE, (d) VC, (e) ethene, and (f) all observations.

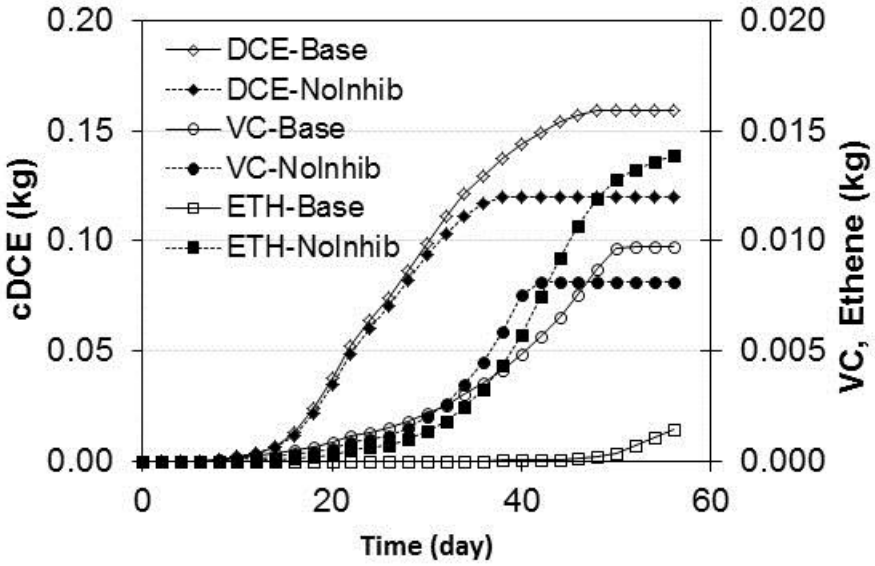

Figure 7. Comparison of simulated cumulative production of *cis*-DCE, VC, and ethene for the base case simulation (open symbols) and no-inhibition (closed symbols) simulation.

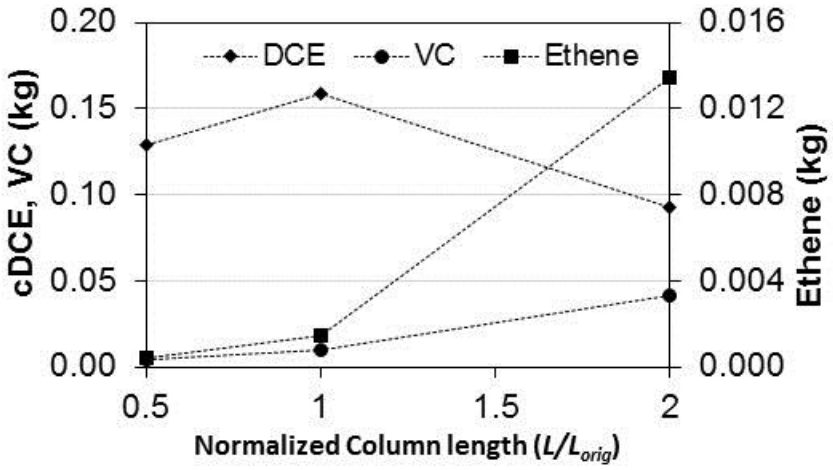

Figure 8. Total mass (kg) of *cis*-DCE, VC, and ethene produced by day 55 for base case, and cases with column length (*L*) reduced by 0.5 and increased by 2.

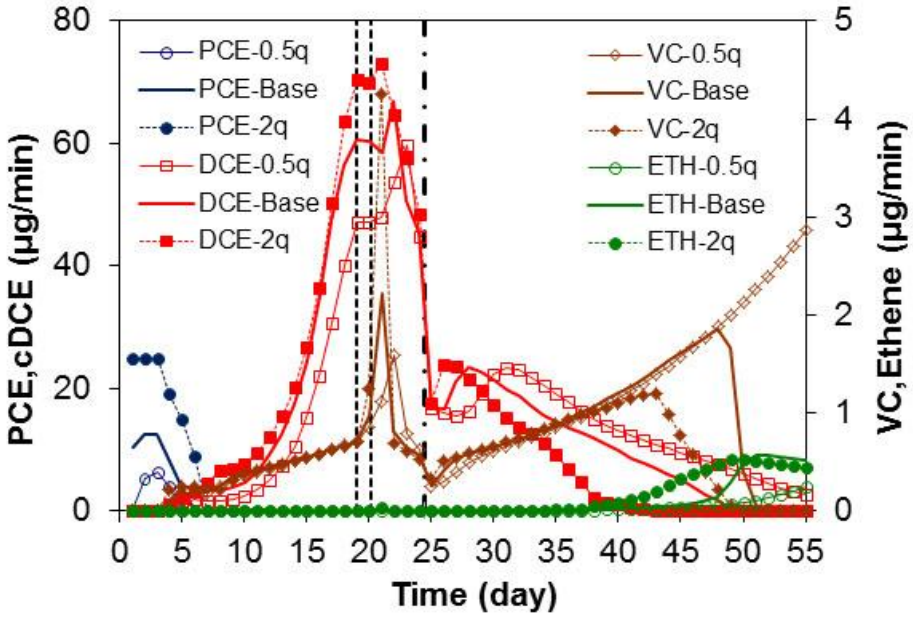

Figure 9. Mass effluent flux (µg/min) of PCE, *cis*-DCE, VC, and ethene for base case (solid line, no symbols), and cases with half (dashed line with open symbols) and double flow rate (q_w) (dashed line with closed symbols).

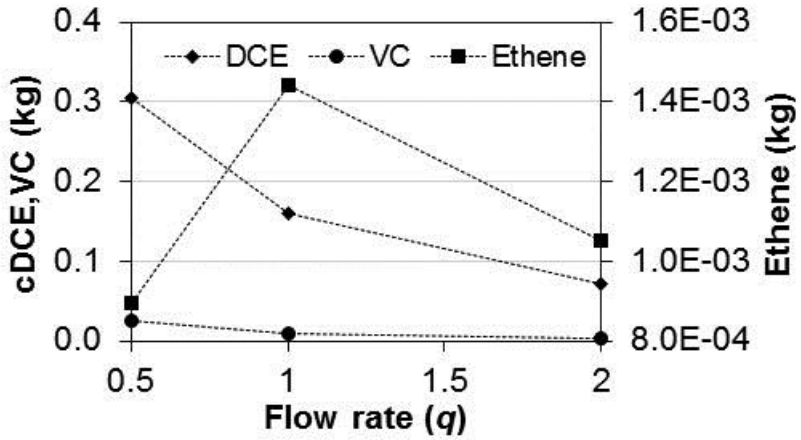

Figure 10. Total mass (kg) of *cis*-DCE, VC, and ethene produced at day 55 for base case, and cases with half and double flow rate.

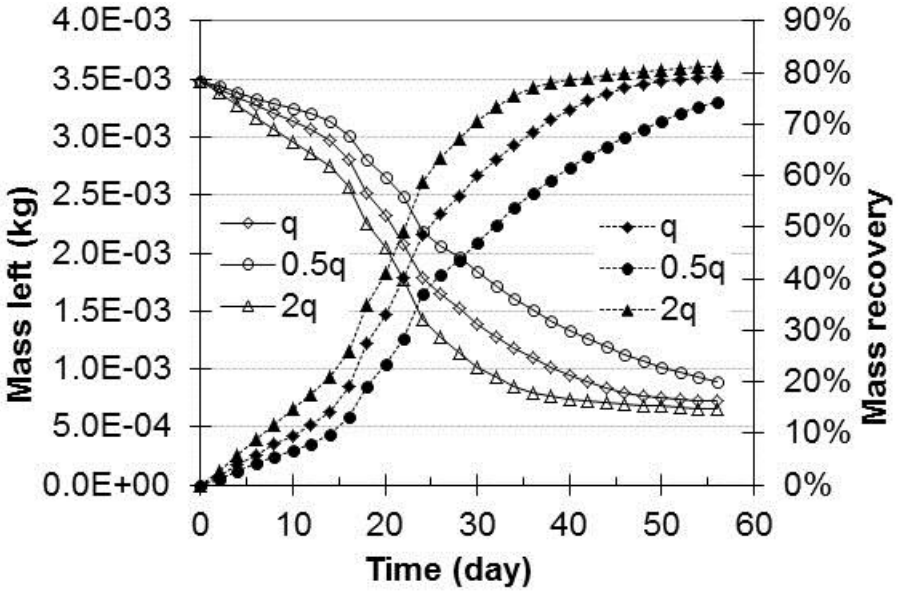

Figure 11. Total chloroethene and ethene mass left in the column (left-hand y-axis, open symbols) and recovered (right hand y-axis, closed symbols) for base case (q_w) (diamonds), and cases with half ($0.5q_w$) (circles) and double ($2q_w$) (triangles) flow rate.